Supplementary Information (SI) for Soft Matter.

Supporting Information: Rounded hard squares confined in a circle

Zhongtian Yuan, Yao Li*

School of Physics and Key Laboratory of Functional Polymer Materials of Ministry of Education, Nankai University, and Collaborative Innovation Center of Chemical Science and Engineering, Tianjin 300071, China

CONTENTS

I. Methods 2

II. Order parameters 3

A. Local bond angular order 3

B. Defect charge 5

III. Chirality 5

IV. Large scale simulation 7

I. METHODS

We performed Monte Carlo (MC) simulations in the isothermal–isobaric (NPT) ensemble. Three types of MC moves were used: translation, rotation, and volume moves. For translation and rotation moves, the acceptance rule is straightforward: any move that results in a particle-edge overlap is rejected, and all other moves are accepted, consistent with the exclusion-driven nature of hard particles.

For volume moves, the acceptance probability is

$$P_{\text{acc}} = \min\left[1,\ \exp\left(-\beta\,\Delta E + \beta p(V' - V) - N\ln\frac{V'}{V}\right)\right], \tag{S1}$$

where ΔE is treated as infinite if the proposed volume change produces any particle overlap, and $\Delta E = 0$ otherwise. Each MC step consists of N translation moves, N rotation moves, and one volume move, where N is the number of particles in the system.

We initialized the simulation at a pressure of $p = 0.5$, with particle centers of mass and orientations assigned randomly. For computational convenience, the initial particle side length was set to $l = 1$; during subsequent volume moves, the particle length was rescaled, which is equivalent to changing the system volume. The radius of the circular boundary R was chosen such that the initial packing fraction satisfied $\eta \approx 0.25$. The packing fraction is computed as:

$$\eta = N\left[a^2 - (\zeta a)^2 + \pi\left(\frac{\zeta a}{2}\right)^2\right]/\pi R^2 \tag{S2}$$

* liyao@nankai.edu.cn

where ζ is the roundness of the particle. When $\zeta = 0$, the particles are perfect squares and $\eta = Na^2/\pi R^2$. When $\zeta = 1$, the particles are disks and $\eta = N\left(\zeta a/2R\right)^2$.

During the simulation, the pressure was increased gradually, with each pressure increment applied after 4×10^4 MC steps. Whenever the packing fraction increased by 0.01, the volume moves were temporarily switched off, and an additional 4×10^4 MC steps were performed to generate a structural snapshot at that packing fraction. After the snapshot was recorded, the volume moves were switched back on, and the pressure was further increased until the next target packing fraction was reached.

After analyzing the structural snapshots at all packing fractions, we find that the system undergoes a transition into a solid phase near a packing fraction of $\eta = 0.75$. The maximum achievable packing fraction depends on the particle roundness and decreases as the roundness increases. At the highest packing fractions reached in the simulations, the system becomes jammed, and we cannot determine whether these configurations correspond to the densest packing. To select a packing fraction that is accessible to systems with all values of particle roundness while maintaining high crystalline quality, we therefore focus on a packing fraction of $\eta = 0.85$.

II. ORDER PARAMETERS

A. Local bond angular order

The Local bond angular order is defined as:$\left(\Psi_n\right)_j = 1/n_j \left|\sum_{k=1}^{n_j} \exp\left(\mathrm{i}n\theta_{jk}\right)\right|$, where θ_{jk} is the angle between an arbitrary axis and the bond formed by particle j and its neighbor k, and n_j represents the number of neighbors for particle j. In this work, neighboring particles are identified by computing the distance between the centers of mass of the particles. For Ψ_4, we select the four nearest neighbors, and for Ψ_6 , the six nearest neighbors. This neighbor selection is not strictly topological, but in the solid phase—where the crystalline quality is high—these neighbors are sufficient to characterize the local ordering around particle j. Near the boundary region, this method may introduce artifacts and slightly reduce the measured order; however, because Ψ_n is a local order parameter, such effects are confined to the outermost layer and do not influence the structural characteristics. Some snapshots of Ψ_4 are shown in S1.

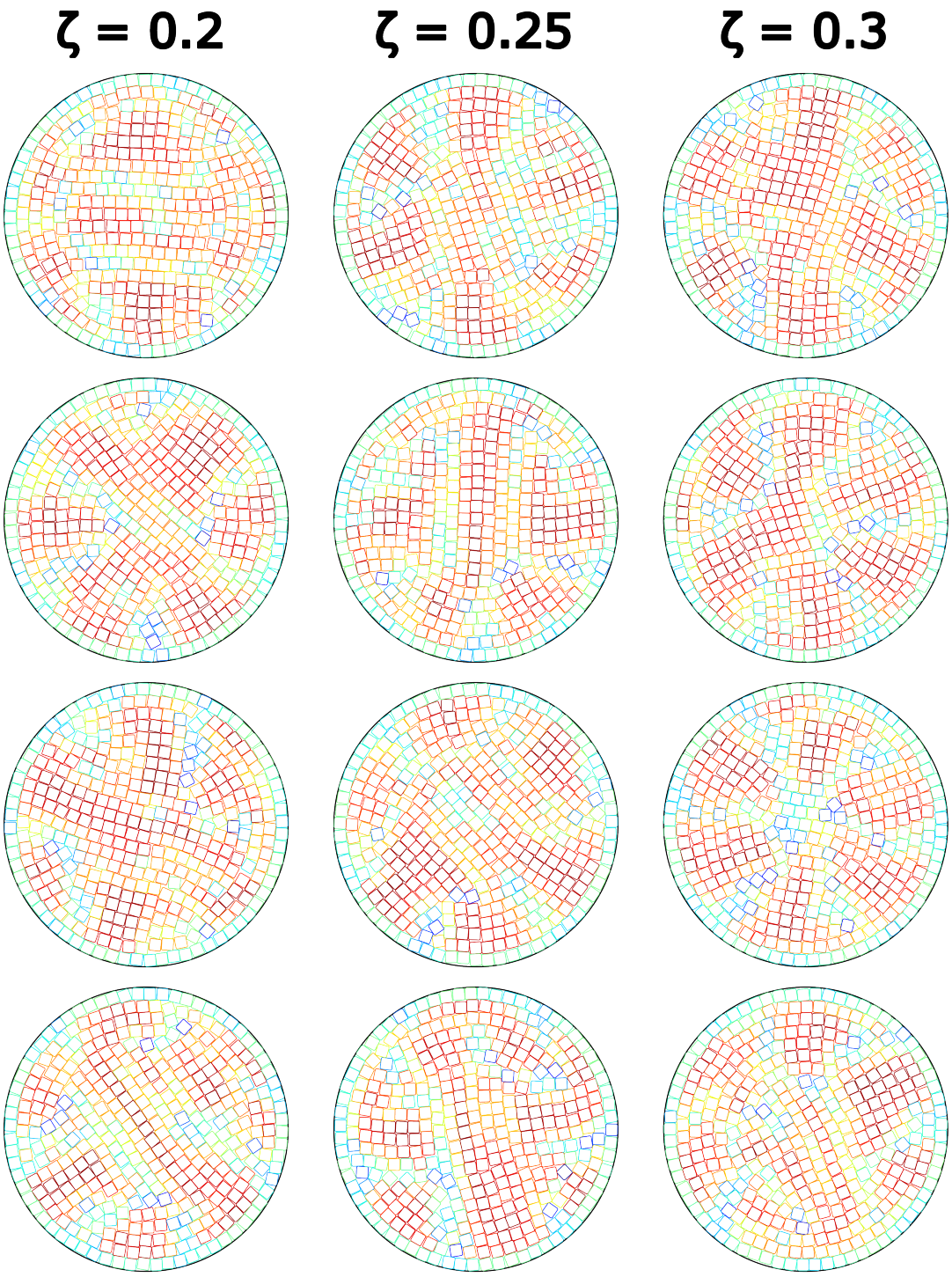

Figure S1. Snapshots of the square–partition structural transition at $\zeta = 0.2$, 0.25, and 0.3. For each column, four independent simulation runs are shown at the same ζ. Near the transition point at $\zeta \approx 0.25$, the system can exhibit either the square structure or the partition structure at all three roundness, and in some cases mixed configurations that are difficult to classify. But the relative occurrence of the partition structure increasing with ζ.

We found that Ψ_6 remains low for $\zeta < 0.5$ and increases rapidly only at high roundness, reflecting the emergence of six-fold local bond order. Therefore, it cannot be used to resolve the detailed differences between the square structure and the partition structure. However, during the square-to-partition transition, the particle arrangement changes in a way that does not produce true six-fold symmetry but still causes Ψ_6 to increase gradually. This slow rise can be interpreted as a signal of the partition transition. For this reason, we use the mean value of Ψ_6 to globally characterize the structure.

B. Defect charge

To compute the defect charge, we adopt the standard winding number approach. A closed loop is constructed around the defect, and the particle orientation is tracked while traversing the loop in either the clockwise or counterclockwise direction. The total rotation angle θ_{rotate} is obtained by summing the incremental orientation changes along the loop. The rotation is defined as positive when the orientation rotates in the same sense as the loop direction and negative when it rotates in the opposite sense. The defect charge is then given by

$$q = \frac{\theta_{\text{rotate}}}{360^\circ}. \tag{S3}$$

For example, a triangular $+1/4$ disclination corresponds to a 90° rotation in the same direction as the loop, while a hexagonal $-1/2$ disclination corresponds to a 180° rotation opposite to the loop direction. This method must be applied within crystalline domains, where particle orientations are well defined; otherwise, the orientation becomes ambiguous along the loop.

III. CHIRALITY

In the partition structure, we find that the system can sometimes develop chirality, appearing as a global twist around the center that forms a spiral-like configuration S2. This behavior arises from the circular confinement, which allows particles to undergo slight rotational adjustments between neighboring layers.

We quantify this helicity-like chirality by measuring how the particle orientation rotates

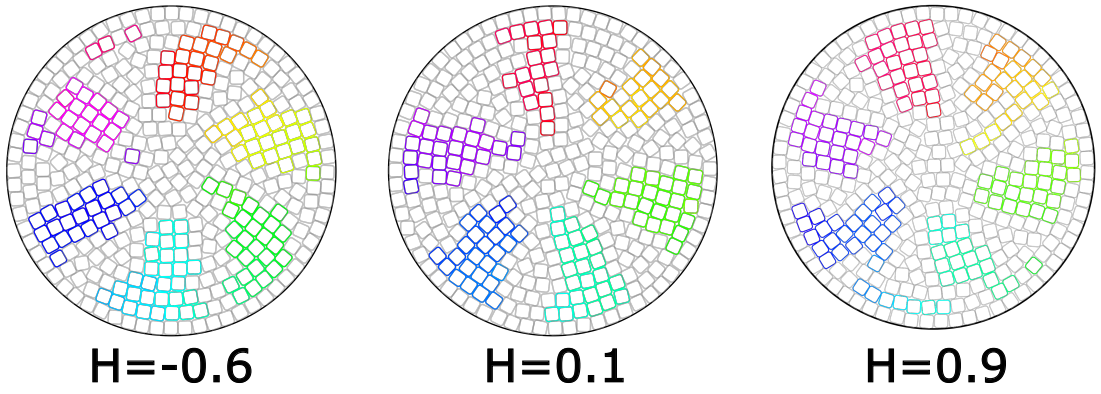

Figure S2. Snapshots of the partition structure exhibiting different chiralities. The chirality H is quantified by the rotational angles (°) of particle orientations, with its detailed definition given in eq. S4. All three snapshots are taken at $\zeta = 0.4$ and packing fraction 0.85.

as the radial distance increases. The chirality is defined as

$$H = 1/N \sum_{i}^{N} (\alpha_j - \alpha_{\text{neighbor}}) \tag{S4}$$

Where α_j is the orientation of particle j and α_{neighbor} is the orientation of its nearest neighbor in the adjacent outer layer. To construct these layers, we classify particles into a series of concentric rings whose radii are given by $r_n = R - (n + 1/2)\, l$, where R is the radius of the circular boundary and l is the particle length. Layer numbers n are counted from the boundary inward because the layering is more pronounced near the boundary. For each particle, the neighbor is identified as the closest particle in the adjacent outer layer. For $H > 0$, the orientations of particles in the inner layers increase relative to those in the outer layers, producing a clockwise spiral twist; for $H < 0$, the orientations decrease, resulting in a counterclockwise spiral, as shown in S2.

We statistically analyze snapshots at $\zeta = 0.10$ and $\zeta = 0.40$ over a packing fraction range from 0.75 to 0.90. The result histogram is shown in S3. For comparison, we also compute a random reference distribution in which each particle retains its radial distance but is assigned a random position and orientation. At $\zeta = 0.4$, where the partition structure forms, the distribution of H closely resembles the random reference, which has a peak at $H = 0$ and symmetric fluctuations around zero. This indicating that the observed helicity behaves primarily as a fluctuation, with the system exhibiting a random bias toward either clockwise or counterclockwise rotation. In contrast, at $\zeta = 0.1$, the square structure promotes stronger

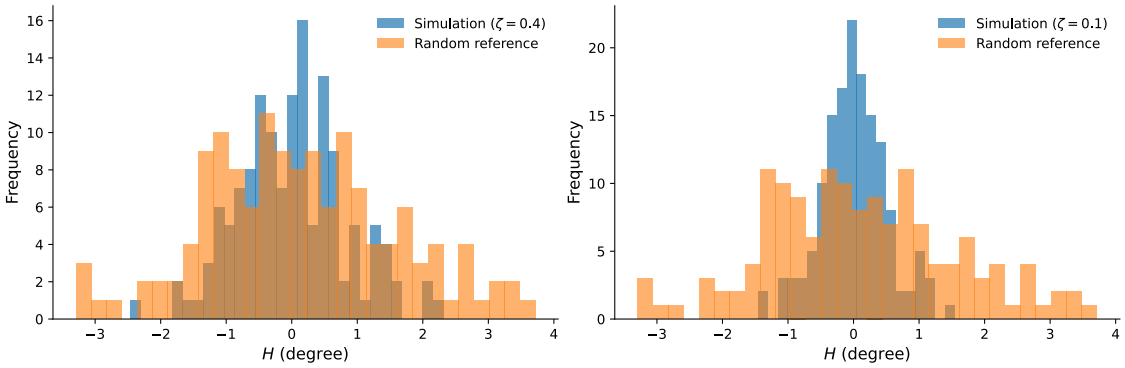

Figure S3. Frequency histograms of the helicity H at $\zeta = 0.1$ and $\zeta = 0.4$. The blue columns represent the simulation data, and the orange columns represent the random reference distribution. Each histogram uses the same number of samples.

orientational alignment within crossover domains, producing a noticeably narrower peak than the random distribution.

In summary, this helicity behaves primarily as a fluctuation rather than a stable state. The typical lifetime of a chiral state is 2×10^5 MC steps, after which the system may untwist or reverse its handedness.

IV. LARGE SCALE SIMULATION

We found that with increasing N, system becomes more flexible. Although it can still distinguish four or six domains in square or partition structure respectively, the shape of the domain becomes less organized, while it is nearly rectangular when $N = 400$.

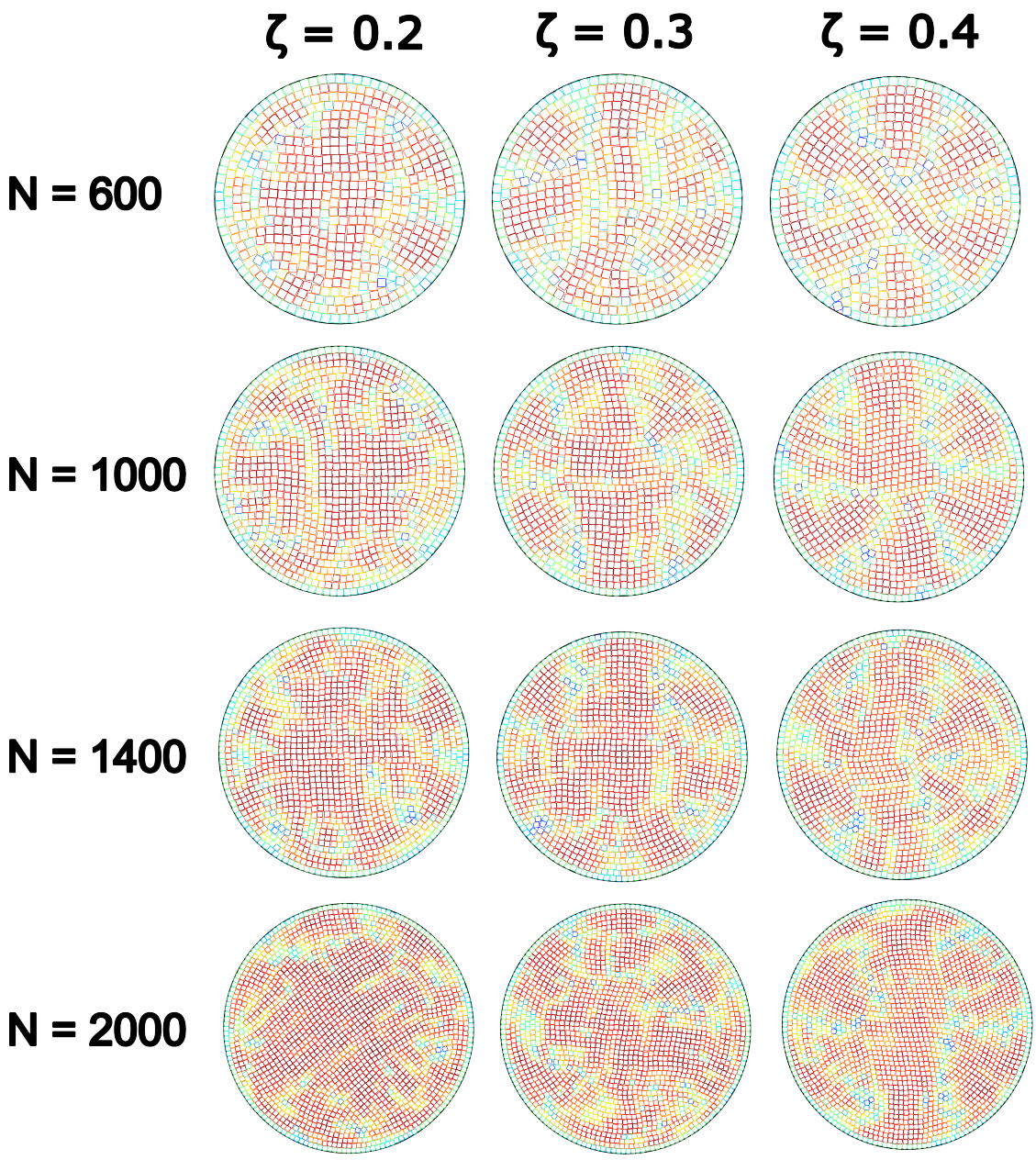

Figure S4. Large scale simulation snapshot at $N = 600$, 1000, 1400, 2000 and $\zeta = 0.2$, 0.3, 0.4. Color coded by local bond angular order Ψ_4.